Transmembrane helices can induce domain formation in crowded model membranes

Domanski, Jan; Marrink, Siewert J.; Schäfer, Lars V.

Published in:
Biochimica et Biophysica Acta-Biomembranes

DOI:
10.1016/j.bbamem.2011.08.021

Publication date:
2012

Biochimica et Biophysica Acta 1818 (2012) 984–994

Contents lists available at SciVerse ScienceDirect

Biochimica et Biophysica Acta

journal homepage: www.elsevier.com/locate/bbamem

Transmembrane helices can induce domain formation in crowded model membranes☆

Jan Domański, Siewert J. Marrink, Lars V. Schäfer *

Groningen Biomolecular Sciences and Biotechnology Institute, and Zernike Institute for Advanced Materials, University of Groningen, Nijenborgh 7, 9747 AG Groningen, The Netherlands

ARTICLE INFO

Article history:
Received 29 June 2011
Received in revised form 27 July 2011
Accepted 15 August 2011
Available online 22 August 2011

Keywords:
Membrane protein
Lipid raft
Crowding
Molecular dynamics
Coarse grained

ABSTRACT

We studied compositionally heterogeneous multi-component model membranes comprised of saturated lipids, unsaturated lipids, cholesterol, and α-helical TM protein models using coarse-grained molecular dynamics simulations. Reducing the mismatch between the length of the saturated and unsaturated lipid tails reduced the driving force for segregation into liquid-ordered (l_o) and liquid-disordered (l_d) lipid domains. Cholesterol depletion had a similar effect, and binary lipid mixtures without cholesterol did not undergo large-scale phase separation under the simulation conditions. The phase-separating ternary dipalmitoyl-phosphatidylcholine (DPPC)/dilinoleoyl-PC (DLiPC)/cholesterol bilayer was found to segregate into l_o and l_d domains also in the presence of a high concentration of TM helices. The l_d domain was highly crowded with TM helices (protein-to-lipid ratio ~1:5), slowing down lateral diffusion by a factor of 5–10 as compared to the dilute case, with anomalous (sub)-diffusion on the μs time scale. The membrane with the less strongly unsaturated palmitoyl-linoleoyl-PC instead of DLiPC, which in the absence of TM α-helices less strongly deviated from ideal mixing, could be brought closer to a miscibility critical point by introducing a high concentration of TM helices. Finally, the 7-TM protein bacteriorhodopsin was found to partition into the l_d domains irrespective of hydrophobic matching. These results show that it is possible to directly study the lateral reorganization of lipids and proteins in compositionally heterogeneous and crowded model biomembranes with coarse-grained molecular dynamics simulations, a step toward simulations of realistic, compositionally complex cellular membranes. This article is part of a Special Issue entitled: Protein Folding in Membranes.

1. Introduction

The traditional view of biological membranes as passive, homogeneous structures [1] has been refined toward the picture of a heterogeneous material in which preferential association of certain lipids, sterols, and proteins can lead to the formation of nanodomains, or rafts [2]. This lateral segregation potential or "patchiness" of the membrane has important implications for many cellular processes, such as the folding of membrane proteins and their self-assembly into functional higher-order clusters [3,4], membrane fusion [5,6], protein trafficking [7], and signal transduction [8–10]. However, despite recent progress [11], the characterization of the structural heterogeneity in vivo remains very challenging, owing to the lack of experimental methods suitable for studying fluctuating nanoscale assemblies of lipids and proteins in living cells with the required spatio-temporal resolution [12–14]. Therefore, model membranes [15–19] and isolated plasma membranes [20–22] are more frequently studied. Under certain conditions, large-scale segregation into macroscopic phases can occur in these systems, which can be visualized with confocal microscopy. In particular, at cholesterol concentrations reminiscent of biological membranes (10–30 mol-%), ternary mixtures of saturated and unsaturated lipids can segregate into coexisting lipid domains of different fluidity, a liquid-ordered (l_o) and a liquid-disordered (l_d) phase.

The exact connection between macroscopic phase separation in model membranes and rafts in cellular membranes is not yet fully understood [23–25]. Recent data suggest that biological membranes are close to a miscibility critical point under physiological conditions, with compositional fluctuations on the <50-nm length scale, which may also be characteristic for lipid nanodomains in vivo [26]. Given its compositional complexity, it is clear that the heterogeneity of biological membranes cannot be ascribed to lipids alone: typical biological membranes are a mix of many different lipid species [27] and are highly crowded with proteins [4,28]. In fact, mass fractions of 50% proteins are not uncommon, and even up to 75% have been reported for mitochondrial membranes [29] (this large fraction is not only due to the TM domains, but also includes the water-soluble parts). Protein–lipid and protein–protein interactions modulate the thermodynamics of lipid mixing [13,30] and thus form the basis of the lateral organization principle in biomembranes [4,31]. Although elastic bilayer theories [32,33] can explain much of the underlying physics, to actually probe these interactions at the level of the individual residues or even atoms

☆ This article is part of a Special Issue entitled: Protein Folding in Membranes.

* Corresponding author.
E-mail address: l.schafer@rug.nl (L.V. Schäfer).

0005-2736/$ – see front matter © 2011 Elsevier B.V. All rights reserved.
doi:10.1016/j.bbamem.2011.08.021

is a challenging task. Molecular dynamics (MD) type computer simulations are powerful tools to achieve that goal [34]. However, the slow lateral diffusion renders the equilibration of heterogeneous multicomponent mixtures of lipids and proteins computationally prohibitively expensive for conventional all-atom simulations. This limitation can be overcome with simplified coarse-grained (CG) models, whose efficiency enables to study biomolecular processes that take place on temporal and spatial scales of tens of nm and μs, respectively [35]. Recent CG simulation studies highlighted the importance of lipid-mediated interactions between membrane proteins [36–43,105]. Reynwar and Deserno studied the effect of a near-critical binary lipid mixture on the clustering of peripheral membrane proteins, represented as simple hexagonal disks, adsorbed onto the bilayer [39]. These simulations provided the first molecularly detailed picture of how composition-mediated protein interactions can decrease the miscibility of the lipid components in a mixture that is close to the critical point.

To provide a closer link to processes occurring in real cell membranes, modeling at a higher level of resolution is warranted. Previously, Risselada and Marrink carried out CG–MD simulations of a lipid bilayer comprised of a ternary mixture of dipalmitoyl-phosphatidylcholine (diC(16:0)PC, DPPC), dilinoleoyl-PC (diC(18:2)PC, DLiPC), and cholesterol in a 0.42:0.28:0.30 molar ratio [44]. The MARTINI CG force field [45,46] was used, in which on average ~4 heavy atoms and associated hydrogens are mapped into a single CG bead. This level of coarse-graining preserves some chemical specificity of the molecules, such as, e.g., the distinction between single and double bonds in the lipid hydrocarbon tails. Starting from an initially random lipid distribution in the bilayer plane, Risselada and Marrink observed spontaneous separation into two fluid domains on the multi-μs time scale at 295 K [44]. The thicker liquid-ordered (l_o) lipid domain mainly comprised of saturated DPPC lipids and cholesterol, whereas the thinner liquid-disordered (l_d) domain was enriched in doubly unsaturated DLiPC lipids and contained less cholesterol. The properties of the formed domain were found to be consistent with experimental data on similar model membranes [47].

Recently, Schäfer and coworkers [48] used CG-MARTINI and all-atom MD simulations to study the partitioning and clustering of transmembrane (TM) α-helices between the l_o and l_d domains in the ternary DPPC/DLiPC/cholesterol bilayer studied by Risselada and Marrink. As TM α-helices, WALP peptides of different length as well as the TM domains of the syntaxin-1A and of the linker for activation of T cells (LAT) proteins were used. Free energy calculations revealed that the enthalpic contribution due to the tight packing of the lipids in l_o drives TM helices into the l_d domains, irrespective of the hydrophobic mismatch between the length of the TM helix and the thickness of the bilayer hydrocarbon region. The partitioning observed in the simulations was confirmed by fluorescence microscopy [48]. The hydrophobic mismatch was found to regulate the clustering of the TM helices into either small and dynamic (small mismatch) or large and static (large mismatch) aggregates. In these simulations, a relatively small number of 12 TM helices were inserted into the bilayer to mimic the diluted conditions in the fluorescence experiments.

However, many biological membranes have a much higher protein content, which modulates the phase behavior. Furthermore, the driving force for phase separation is rather strong in the ternary DPPC/DLiPC/cholesterol simulation system, in line with a high line tension of 14 ± 2 pN at the domain boundary interface [49]. The doubly unsaturated DLiPC lipids form a strongly disordered l_d domain, while the almost complete depletion of unsaturated lipids leads to a high degree of order in the l_o domain [44]. Experiments with model membranes reported smaller line tensions of the order of a few pN [17,50].

The aim of the present study is threefold: First, we characterized lipid compositions with a reduced driving force for segregation, which in this respect more closely resemble the typical model membrane systems studied experimentally. Second, we investigated the effect of a high concentration of TM α-helices on the mixing behavior of the lipids, and show how the addition of TM helices that preferentially bind to one lipid component can amplify non-ideal lipid mixing and bring the system closer to a miscibility critical point. Our third aim was to go beyond individual TM helices and study a realistic membrane protein. We therefore simulated the l_o/l_d partitioning of a multi-domain protein, the 7-TM helix protein bacteriorhodopsin (bR).

2. Methods

2.1. Molecular dynamics simulations

All simulations were carried out with the Gromacs (version 4.0.5) MD package [51]. The MARTINI coarse grained (CG) force field [45,46] was used, together with a 20-fs integration time step. In MARTINI, particles that are not directly connected by bonds interact through a Lennard–Jones (LJ) 12,6-potential. The LJ interaction strength between beads, ε_{LJ}, can adopt nine discrete values ranging from 5.6 kJ/mol to 2.0 kJ/mol. Coulomb interactions between (non-bonded) explicit charges, such as zwitterionic phosphocholine headgroups or charged amino acid sidechains, are treated by a Coulomb potential that is screened with a relative dielectric constant of $\varepsilon_r = 15$. The LJ and Coulomb potentials are smoothly shifted to zero between 0.9 nm and 1.2 nm and 0 and 1.2 nm, respectively. Constant particle number, pressure, and temperature (NpT) ensembles were simulated within periodic boundary conditions. Semi-isotropic pressure coupling was applied by separately coupling the lateral (xy) and normal (z) directions to a pressure bath ($p = 1$ bar, $\tau_p = 3$ ps, $\chi = 3 \cdot 10^{-5}$ bar^{-1}), yielding a tensionless bilayer. Temperature was maintained by coupling to a heat bath at 295 K, the chain melting temperature of a pure DPPC bilayer in the MARTINI model [52], using a Langevin thermostat (SD integrator in Gromacs) with a friction constant of $\zeta = 0.2$ ps^{-1} ($\tau_T = 5$ ps). The local Langevin thermostat produces configurations in the canonical ensemble, but the diffusion depends on ζ [53,54]: a small ζ does not substantially disturb Hamiltonian dynamics, whereas a large ζ results in a friction that is higher than the internal friction due to the collisions of the particles and thus quenches diffusion. To choose a proper ζ for our simulations, we carried out CG-MARTINI simulations of a DPPC bilayer at 323 K, and compared the diffusion coefficients obtained with the local Langevin thermostat and the velocity rescaling thermostat of Bussi and coworkers [55]. A small Langevin friction constant of $\zeta = 0.2$ ps^{-1} was found to sufficiently remove excess heat from the system, while it yields diffusion coefficients that are only about 10% lower than with velocity rescaling (with $\tau_T = 0.3$ ps), indicating that the dynamics is close to the Hamiltonian regime.

2.2. Molecular models

Molecules considered in this study are the saturated lipids dipalmitoyl-phosphatidylcholine (diC(16:0)PC, DPPC), dimyristoyl-PC (diC(14:0)PC, DMPC), and didecanoyl-PC (diC(10:0)PC, DDPC), the unsaturated lipids dilinoleoyl-PC (diC(18:2)PC, DLiPC), palmitoyl-linoleoyl-PC (C(16:0)-C(18:2)PC, PLiPC), and dioleoyl-PC (diC(18:1)PC, DOPC), as well as cholesterol, and the model transmembrane helix WALP23 (AW_2L-$(AL)_8$-W_2A). Fig. 1 shows the MARTINI CG representations of the DPPC, DLiPC, cholesterol, and WALP23 molecules. Apolar hydrophobic C_1-type beads were used to model the saturated segments of the hydrophobic lipid tails, whereas we used slightly less hydrophobic C_4-type beads for the unsaturated segments, reflecting the larger polarizability of sp^2-hybridized carbon atoms. The C_1–C_1 and C_4–C_4 interactions were modeled by a LJ interaction with $\varepsilon_{C1-C1} = \varepsilon_{C4-C4} = 3.5$ kJ mol^{-1}, whereas the C_1–C_4 LJ interaction was slightly weaker, $\varepsilon_{C1-C4} = 3.1$ kJ mol^{-1}. This difference contributes to the driving force for segregation of the different lipid species. The full LJ interaction matrix of the MARTINI force field can be found in Ref. [45]. Palmitoyl and linoleoyl hydrocarbon tails were modeled with 4 beads, oleoyl tails with 5, myristoyl tails with 3, and decanoyl

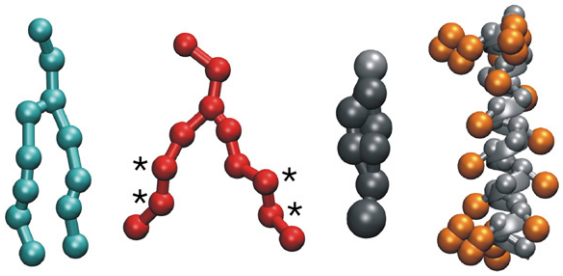

Fig. 1. MARTINI coarse-grained models of DPPC, DLiPC, cholesterol, and the α-helical WALP23 peptide (left to right). The DPPC and DLiPC lipids are shown in cyan and red, respectively; unsaturated (C_4-type) beads are marked with an asterisk. The cholesterol ring and exocyclic hydrocarbon chain are shown as small and large gray beads, respectively, and the headgroup is represented by a small light gray bead. The backbone of WALP23 is shown in light gray and the sidechains in orange.

tails with 2 beads, respectively. The bending rigidity of the lipids was controlled by a harmonic angle potential between three consecutive beads. For saturated hydrocarbon tails, an equilibrium angle of $\theta_0 = 180°$ and a force constant of $k_a = 25$ kJ mol^{-1} rad^{-2} were used. The kink in singly unsaturated oleoyl tails was described by an angle potential with $\theta_0 = 120°$, $k_a = 45$ kJ mol^{-1} rad^{-2}, which yields angle distributions matching those from atomistic simulations [45]. For the more flexible polyunsaturated tails, $\theta_0 = 100°$, $k_a = 10$ kJ mol^{-1} rad^{-2} and $\theta_0 = 120°$, $k_a = 45$ kJ mol^{-1} rad^{-2} between the upper and terminal three beads, respectively, were used. These parameters were derived from atomistic simulations of stearoyl-docosahexaenoyl-phosphatidylcholine (SDPC) bilayers [56] and were applied in previous simulations in our group [44,57,58] and by others [59,60]. The α-helicity of the WALP peptides (Fig. 1) was imposed during the CG simulations through dihedral potentials between four consecutive backbone beads, with an equilibrium dihedral angle of 60° and a force constant of 400 kJ mol^{-1} [46]. The N- and C-termini of the peptides were capped with uncharged P_3-type beads. Lipid topologies, scripts to generate generic protein topologies, and force field parameters can be downloaded from our website www.cgmartini.nl.

2.3. System set-up

The lipid bilayer simulated by Risselada and Marrink [44] served as a platform for our simulations. This lipid bilayer comprised of 828 DPPC, 540 DLiPC, and 576 cholesterol molecules (1944 molecules in total), solvated by 12,600 CG water beads (one CG bead represents 4 atomistic water molecules in the MARTINI force field). The x,y,z-dimensions of the simulation box were about 22×22×7 nm. To reduce the line tension in this system, either the saturated component (DPPC) was replaced by shorter tail lipids (DMPC, DDPC), or the poly-unsaturated component (DLiPC) was replaced by more saturated lipids (PLiPC, DOPC). To change the saturated lipid component from DPPC to DMPC, the terminal bead from each DPPC hydrocarbon tail was removed. Changing the unsaturated lipids from DLiPC to PLiPC did not require removing or adding beads, since both lipids are comprised of the same number of beads in the MARTINI CG representation. The hydrocarbon tails of DOPC, however, are modeled by 5 beads in MARTINI [45]. Thus, to replace DLiPC by DOPC, beads had to be added. This was done by extending the box in the direction normal to the bilayer (z-axis) by 1 nm, removing the water, centering the membrane in the new box, and translating the upper and lower leaflets by +0.5 nm and −0.5 nm, respectively, along the z-axis. Then, the 5th tail beads were added to the unsaturated lipids, placed at a z-position 0.47 nm below (for the upper leaflet) or above (for the lower leaflet) the 4th tail beads of the respective lipids. The bilayer was then re-hydrated with 12,600 CG water beads (taking care that no water beads were added in the hydrocarbon region of the bilayer), energy minimized with 1000 steps of steepest descent, and equilibrated with harmonic position restraints on the phosphate headgroup beads (force constant 1000 kJ mol^{-1} nm^{-2}) for 20 ns prior to the production simulation. To probe the role of cholesterol in the domain formation, additional simulations with 6, 10, 17, and 24 mol-% cholesterol were set-up by removing cholesterol from the original bilayer (containing 30 mol-% cholesterol); care was taken that the same number of cholesterol molecules was removed from both leaflets.

To simulate how TM helices can modulate the phase behavior, model TM helices (WALP23) were inserted into the lipid bilayers by overlaying the lipid bilayers with a lateral grid of helices (regularly distributed on the grid and not tilted with respect to the membrane normal), removing all overlapping lipid molecules, and energy minimizing the system (1000 steps steepest descent). While inserting 12 TM helices did not significantly reduce the number of lipids in the bilayer, inserting 64 TM helices yielded a bilayer with 490 DPPC, 252 DLiPC, and 356 cholesterol molecules, in addition to the 64 WALP23 peptides. Thus, comparatively more unsaturated lipids than saturated lipids were removed (due to the larger area per lipid of the former), which would have resulted in a rather small number of unsaturated lipids. Thus, we randomly replaced 90 saturated lipids by unsaturated lipids, taking care that the number of saturated and unsaturated lipids is the same in both leaflets. This yielded a simulation system with 400 DPPC, 342 DLiPC (or PLiPC), and 356 cholesterol molecules. For bR, a single protein was inserted into the bilayer, and all molecules that had at least one bead within 0.2 nm of the protein were removed from the system, followed by energy minimization (1000 steps steepest descent). This yielded a bilayer with 800 saturated lipids, 498 unsaturated lipids, and 540 cholesterols. For bR, the X-ray crystal structure at 0.155 nm resolution, PDB ID: 1C3W [61], was used as the starting structure for our simulations. For generating the CG topology, the secondary structure elements were assigned with the program DSSP [62]. The structure was converted into its CG representation using the MARTINI mapping. The retinal moiety was removed from the structure, as it is buried inside the protein and is not expected to have an influence on the l_o/l_d partitioning. All backbone beads within a distance range between 0.5 and 0.9 nm were connected with harmonic bonds (force constant 500 kJ mol^{-1} nm^{-2}) to ensure that the structure could not deviate strongly from the X-ray crystal structure during the CG–MD simulations; this combination of the distance range and force constant was chosen based on a recent systematic study on combining the MARTINI force field with an elastic network [63]. All simulations were started from a configuration in which the lipids were laterally mixed, i.e., a non-phase-separated configuration, unless noted otherwise. All simulations are summarized in Table 1.

2.4. Analysis

2.4.1. Fraction of lipid–lipid contacts

To characterize the time course of the mixing behavior, we calculated the number of contacts between saturated and unsaturated PC lipids in the ternary mixtures, divided by the total number of contacts between unsaturated lipids with all other PC lipid molecules in the simulation system, i.e., saturated and unsaturated PC lipids. Two lipids were considered to be in contact if the distance between their phosphate headgroup beads was within 1.1 nm, which includes the solvent-separated peak in the radial distribution function. A 0.8-nm cutoff yielded very similar results (not shown).

2.4.2. Line tension

The line tension at the domain boundary interface, σ, was calculated from the pressure tensor according to $\sigma = {}^1/_2\langle L_\perp L_z(p_\perp - p_{||})\rangle$, where $p_\perp$ and $p_{||}$ are the pressure tensor components perpendicular and parallel to the interface (in the bilayer plane), respectively, $L_\perp$ and L_z are the box dimensions perpendicular to the interface and along the bilayer normal, respectively, and factor 1/2 takes into account that there are

Table 1
Overview of simulations.

Simulation system (molar ratio)	Simulation time [μs]	Mixing[a]	Line tension [pN]
Ternary mixtures of saturated and unsaturated lipids with cholesterol			
DPPC/DLiPC/CHOL[b] (828:540:576)	10	Phase separation	14 ± 2
DMPC/DLiPC/CHOL (828:540:576)	10	Phase separation	4 ± 2
DDPC/DLiPC/CHOL (828:540:576)	5	Non-ideal (2 nm)	–
DPPC/DOPC/CHOL[c] (828:540:576)	6	Non-ideal (2.5 nm)	–
DPPC/PLiPC/CHOL (828:540:576)	6	Non-ideal (2.5 nm)	–
Cholesterol depletion			
DPPC/DLiPC/CHOL (828:540:432)	10	Phase separation	12 ± 2
DPPC/DLiPC/CHOL (828:540:288)	10	Phase separation	8 ± 2
DPPC/DLiPC/CHOL (828:540:144)	10	Phase separation	2 ± 2
DPPC/DLiPC/CHOL (828:540:86)	15	Phase separation	1 ± 3
Quaternary mixtures with TM proteins			
DPPC/DLiPC/CHOL/WALP23 (400:342:356:64)	20	Phase separation	18 ± 3[d]
DPPC/DLiPC/CHOL/WALP23[e] (828:540:576:12)	20	Phase separation	22 ± 5
DPPC/PLiPC/CHOL/WALP23 (400:342:356:64)	20	Critical (6 nm)	–
DPPC/PLiPC/CHOL/WALP23 (828:540:576:12)	20	Non-ideal (3.5 nm)	–
DPPC/DLiPC/CHOL/bR (800:498:540:1)	9	Phase separation	15 ± 3
DMPC/DLiPC/CHOL/bR (800:498:540:1)	9	Phase separation	5 ± 3

[a] The length scale of non-ideal mixing is given (between parentheses).
[b] Ref. [49].
[c] In addition, a 15-μs simulation at 285 K was carried out that was initiated in the phase-separated state, and a four times larger system (7776 lipids) was simulated for 3.2 μs.
[d] Obtained from an additional 12-μs simulation with 490 DPPC, 252 DLiPC, 356 CHOL, and 64 WALP23 molecules, in which a striped domain pattern formed.
[e] Ref. [48].

two interfaces in the periodic simulation box. The brackets denote an ensemble average, which was taken over the second half of the simulations. The statistical error was calculated from the pressure fluctuations using a block averaging procedure, as described in Ref. [64] and implemented in the g_analyze tool of Gromacs.

2.4.3. Radial distribution functions

The radial distribution functions (RDFs) between phosphate headgroup beads in the bilayer plane were calculated by averaging over the last 1 μs of the simulations. The bilayer leaflets were analyzed separately, and a bin-width of 0.05 nm was used. To quantify the preferential solvation of the different lipid species in the ternary mixtures, we calculated the Kirkwood–Buff integrals [65] according to

$$G_{ij} = 2\pi \int_0^{R_c} r \cdot \left[g_{ij}(r) - 1 \right] dr,$$

where $g_{ij}(r)$ is the 2-dimensional radial distribution function between the molecules i and j. The integration was carried out up to a cut-off of $R_c = 3$ nm, which is about the length-scale of non-ideal mixing in the analyzed systems (see Results and discussion). We then defined the preferential solvation parameter, δ, between saturated and unsaturated lipid components as $\delta = (G_{sat-sat} + G_{unsat-unsat})/2 - G_{sat-unsat}$. The deviation of δ from 0 describes the degree of non-ideal mixing.

2.4.4. Dynamical properties

We calculated the mean square displacement (MSD) of the molecules in the membrane plane, $MSD = \langle |r(t+t_0) - r(t_0)|^2 \rangle$, where r is the center of mass vector of the molecule, and the time window averaging was done over all time origins t_0. The last 4 μs of the simulations was analyzed; for the lipids, the two leaflets of the bilayer were analyzed separately. The overall center of mass motion was removed. Anomalous diffusion, or subdiffusion, is characterized by a nonlinear dependence of the MSD on time, i.e., MSD $\sim t^{\alpha}$ with $\alpha < 1$. The anomaly exponent, α, was obtained from the local slope of the MSD curves according to $\alpha = d(\ln(MSD))/d(\ln(t))$, with 10-ns intervals for the linear fits.

To compare CG simulation times to experimental time scales, a possible speed-up in the simulations has to be taken into account: the energy landscape of CG models is smoother than that of atomistic models due to the removed friction from the motion of the individual atoms, and the energy barriers may also be smaller than at the fully atomistic level. For the MARTINI CG model, an effective speed-up of about a factor 4 was found for the lateral diffusion of DPPC lipids in a bilayer at 323 K [45]. Recently, we systematically compared simulated and experimentally measured lateral diffusion coefficients of WALP TM peptides in mono-unsaturated PC lipid bilayers of different thickness. The lateral diffusion coefficients obtained from our MARTINI CG simulations were about a factor of 4 higher than those from the fluorescence correlation spectroscopy experiments [66], suggesting that a similar speed-up may also be applicable in the present case. However, the exact time-conversion factor is expected to vary with the composition and state point of the system, and may even be different for the different components in a multi-component mixture [67]. Since there are no experimental diffusion coefficients available for the systems studied here, we did not scale time and report plain simulation times in this work.

3. Results and discussion

This part is organized as follows: in Sections 3.1 and 3.2 we describe the results for ternary lipid systems, either with a reduced mismatch between the l_o and l_d domains (Section 3.1) or with a reduced concentration of cholesterol (Section 3.2). Sections 3.3 and 3.4 concern quaternary mixtures including model TM helices. We describe both the partitioning (Section 3.3) and dynamics (Section 3.4) of these mixtures. In Section 3.5 results obtained for a real membrane protein (bacteriorhodopsin) are presented.

3.1. Reducing the mismatch between the saturated and unsaturated lipids reduces the driving force for phase separation

Cholesterol prefers saturated lipids over unsaturated lipids, leading to condensation into the l_o phase with increased orientational order of the (saturated) lipid hydrocarbon tails to optimize the packing with cholesterol [68]. The concomitant increase in the mismatch between the effective lengths of the saturated and unsaturated hydrocarbon tails contributes to the segregation into l_o and l_d phases in ternary mixtures [69]. Hence, replacing DPPC in l_o by lipids with shorter hydrocarbon tails and/or DLiPC in l_d by less strongly unsaturated lipids (that thus effectively have longer tails) is expected to reduce the driving force for phase separation.

3.1.1. Ternary DMPC/DLiPC/cholesterol system

First, we investigated a ternary mixture of saturated PC lipids with short hydrocarbon tails, DLiPC, and cholesterol (0.42:0.28:0.30 molar ratio). We used a saturated phospholipid with three hydrocarbon CG beads in each tail (see Methods), which will be referred to as diC(14:0)PC (dimyristoyl-PC, DMPC); however, it generally represents saturated lipids with a tail length of 12–15 carbon atoms in the MARTINI CG force field. Experimentally, ternary mixtures of DMPC,

DOPC, and cholesterol can undergo macroscopic phase separation in giant unilamellar vesicles [19]. Since the doubly unsaturated DLiPC used in our simulations increases the tendency to demix as compared to the singly unsaturated DOPC, our DMPC/DLiPC/cholesterol simulation system is expected to be able to phase-separate as well.

Fig. 2 shows that the DMPC (cyan) and DLiPC (red) lipids in the ternary mixture segregate into two distinct domains, which form a striped pattern via the periodic boundaries of the simulation box. To characterize demixing, we calculated the fraction of DLiPC-DMPC contacts (see Section 2.4). Fig. 2B shows that the fraction of DLiPC-DMPC contacts decreases at the beginning of the simulation and stabilizes after about 5 μs, indicating that the phase separation process is completed.

As expected, the l_o and l_d domains are enriched in DMPC and DLiPC lipids, respectively (Fig. 2C). Analyzing the equilibrium compositions at the core of the bulk domains formed at the end of the simulation shows that the l_o domain is almost completely depleted of unsaturated DLiPC lipids (<1 mol-%) and comprises of about 60% DMPC and 40% cholesterol, whereas the bulk l_d domain contains about 85% DLiPC, 5% DMPC, and 10% cholesterol. In the corresponding bilayer containing DPPC as the saturated component, the composition of the l_o domain is also about 60% DPPC and 40% cholesterol, whereas the l_d domain comprises of about 89% DLiPC, 3% DPPC, and 8% cholesterol. These latter values deviate slightly from the ones reported by Risselada and Marrink [44] and were obtained by extending the previous simulations, in which the phase separation process was not finished [49].

To more quantitatively characterize the phase separation behavior, we calculated the line tension at the domain boundary interface from the pressure tensor (see Section 2.4). The obtained line tension of $\sigma = 4 \pm 2$ pN is significantly smaller than $\sigma = 14 \pm 2$ pN in the corresponding DPPC/DLiPC/cholesterol system [49], see Table 1. Since the compositional differences between the bulk domains in the DMPC- and DPPC-containing ternary systems are rather minor, the significantly smaller line tension in the DMPC-containing bilayer is mainly attributed to the reduced thickness mismatch due to the similar effective lengths of the hydrocarbon tails of DMPC and DLiPC. Fig. 2D compares the thickness profiles of the DMPC- and DPPC-containing bilayers (solid and dashed line, respectively). In the DMPC-containing bilayer, the distances between the phosphate headgroups, d_{PP}, are 3.88 and 3.63 nm in the l_o and l_d domains, respectively, a difference of only 0.25 nm. By contrast, the l_o domain in the DPPC-containing bilayer is much thicker, 4.57 nm. Thus, as expected, the shorter DMPC lipid strongly reduces the thickness mismatch between the l_o and l_d domain as compared to DPPC, leading to the reduced line tension.

It takes significant time to equilibrate the compositions of the two domains and the domain boundary interface, a process that is driven by the slow lateral diffusion of the lipids. To assess whether our simulations are long enough to yield equilibrated configurations, we calculated the mean square displacement (MSD) of the lipids in the bilayer plane (see Section 2.4). During the 10 μs of simulation time, the DMPC lipids sampled a root mean square distance of $(\mathrm{MSD})^{1/2} \approx 18$ nm, which is larger than the stripe-width of the domains of ~10 nm (Fig. 2). Alternatively, we can estimate the diffusive relaxation rate, which for the striped l_o/l_d pattern of the membrane is given by $r_{\mathrm{diff}} = (D_{\mathrm{lat}}\, k^2)$, assuming that the composition modulation of wavelength $\lambda = 2\pi/k$ decays exponentially with a time constant $\tau_{\mathrm{diff}} = (r_{\mathrm{diff}})^{-1}$ [39]. With $\lambda \approx 20$ nm (twice the stripe-width) and a lateral diffusion coefficient of $D_{\mathrm{lat}} \approx 8\ \mu\mathrm{m}^2\ \mathrm{s}^{-1}$, $\tau_{\mathrm{diff}} \approx 1.5$ μs is obtained. Taken together, these considerations indicate that our simulations are long enough for equilibration of the lateral composition.

3.1.2. Ternary DDPC/DLiPC/cholesterol system

The above results show that ternary DMPC/DLiPC/cholesterol mixtures can undergo phase separation, and that the reduced mismatch between the lengths of the saturated and unsaturated hydrocarbon tails leads to a reduced line tension as compared to the corresponding system containing DPPC as the saturated component. To probe the effect of even shorter saturated lipids, we carried out a simulation with saturated lipids containing only 2 beads per hydrocarbon tail. This lipid is referred to as di(C10:0)PC (didecanoyl-PC, DDPC), but generally represents lipids with saturated tails of 8–11 carbon atoms in the MARTINI force field. Ternary mixtures of such short saturated lipids, longer-tail unsaturated lipids, and cholesterol have not been characterized experimentally, probably also due to the fact that very short lipids do not form stable lamellar phases on their own. In our simulations, the lamellar state is stabilized by the periodic boundary conditions.

As shown in Fig. 3 (panels A–C), our simulations predict that the ternary DDPC/DLiPC/cholesterol mixture does not phase separate at 295 K. The snapshot after 5 μs of CG–MD simulation (Fig. 3A) shows that the different lipid species are mixed, consistent with the almost

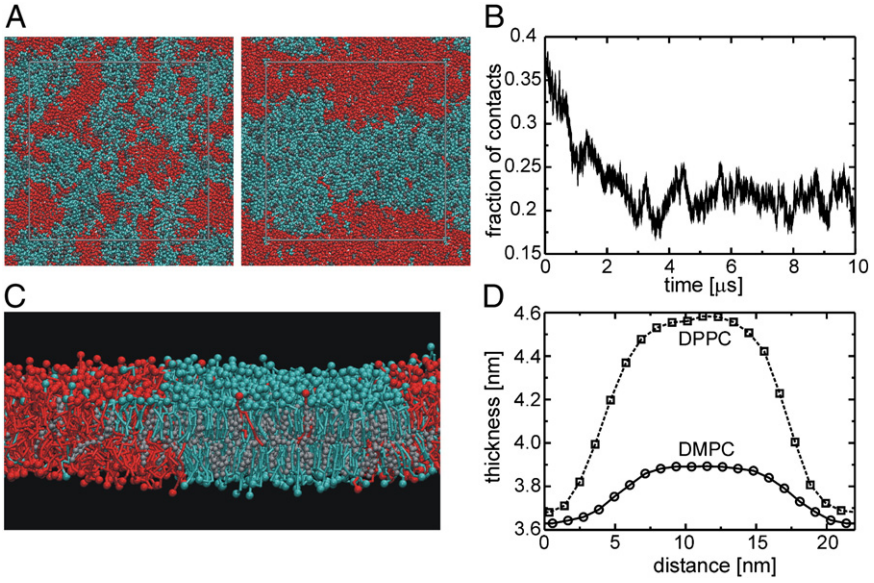

Fig. 2. Phase separation of ternary DMPC/DLiPC/cholesterol lipid bilayer in CG–MD simulation. A) Snapshots (view perpendicular to the membrane plane) at the beginning of the simulation (left) and after 10 μs (right). DMPC molecules are colored cyan, DLiPC red, cholesterol gray. The simulation box is shown in gray, water is not shown for clarity. B) Fraction of DLiPC–DMPC contacts over time. C) Side view of the phase separated system, showing the l_o (cyan) and l_d (red) lipid domains. D) Thickness profile along the lateral dimension perpendicular to the domain boundary interface for DMPC/DLiPC/cholesterol bilayer (solid line), and for the corresponding system containing DPPC as a saturated component (dashed line).

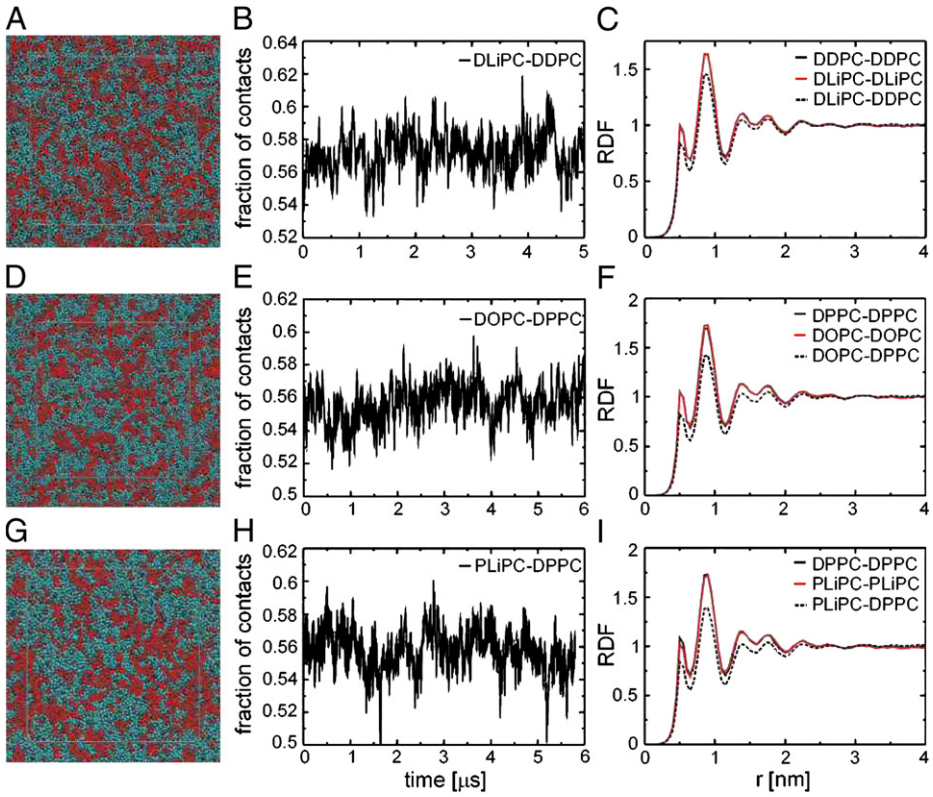

Fig. 3. Ternary mixtures of saturated and unsaturated PC lipids with cholesterol showing non-ideal mixing but no large-scale phase separation. A–C) DDPC/DLiPC/cholesterol, D–F) DPPC/DOPC/cholesterol, G–I) DPPC/PLiPC/cholesterol. Left panels: Snapshots (top view) at the end of the CG–MD simulations. The saturated lipids are colored cyan, unsaturated lipids red, and cholesterol gray. Middle panels: Fraction of contacts between unsaturated and saturated lipids over time. Right panels: Radial distribution functions.

unchanged fraction of DLiPC–DDPC contacts during the course of the simulation (Fig. 3B). The hydrocarbon tails of DDPC are too short to strongly interact with the extended cholesterol ring moiety, and cholesterol is thus not able to order the short saturated tails sufficiently for forming an l_o phase. To more closely characterize the degree of mixing and the spatial order, we calculated the radial distribution functions (RDFs) between phosphate headgroup beads in the bilayer plane. The RDFs (Fig. 3C) are typical for a membrane in the fluid phase, with a rapid decay of the lateral order within about 3 nm. The different amplitudes of the cross- (dashed line) and auto-correlation (solid lines) functions also show that within a distance range extending up to about 2 nm, each lipid species is preferentially surrounded by its own kind, indicating non-ideal mixing on this length scale (see also Table 1). Within the simulation, the lipids sample a root mean square distance of about 25 nm, indicating that the simulation time of 5 μs is sufficient in this case.

3.1.3. Ternary DPPC/DOPC/cholesterol system

Next, instead of changing the saturated lipids of the ternary mixture, we altered the unsaturated lipid component. The initial choice for DLiPC was motivated by the fact that the doubly unsaturated lipids enhance the driving force for phase separation, while yielding domain properties similar to those observed in DPPC/DOPC/cholesterol bilayers that are more frequently studied experimentally [17–19,47]. However, when we replaced DLiPC by DOPC in our simulations, separation into two macroscopic phases was not observed (Fig. 3, panels D–F), although the lipids non-ideally mixed on a length scale up to ~2.5 nm, similar to the DDPC/DLiPC/cholesterol mixture. A similar result was obtained in an additional simulation that was started from a demixed configuration, even at a lower temperature of 285 K (not shown). This apparent disagreement with experiments could either reflect a deficiency of the CG model used, or be due to finite size effects: a very small line tension would mean that the slow, large-amplitude fluctuations of the domain boundary interface may lead to an ill-defined interface due to the limited simulation time scale and size of our simulation box. To test whether such finite size effects could play a role, a four times larger lipid bilayer was generated by repeating the previous simulation system in both lateral dimensions, yielding a simulation box with lateral dimensions of about 44 nm. Although the simulation time of 3.2 μs that we could afford for this large bilayer is too short for the lipids to fully sample the bilayer plane, we expect that the onset of demixing would be observable already on this time scale (Fig. 2B). However, the mixing behavior of this larger bilayer was very comparable to the smaller system (not shown). Another result that speaks against finite size effects is the simulation of a ternary DPPC/DLiPC/cholesterol mixture with 6 mol-% cholesterol, which does undergo phase separation on the 22-nm length scale of the simulation box (see Section 3.2), although the line tension is only ~1–2 pN (Table 1). Thus, we conclude that the reason for the disagreement with experiments is due to approximations underlying the CG force field. Apparently, a single double bond per hydrocarbon tail, represented by a C_4-type bead and the appropriate angle potential (see Methods), is not sufficient to yield lipid phase separation. The DOPC model is currently being optimized to improve its behavior.

3.1.4. Ternary DPPC/PLiPC/cholesterol system

Instead of distributing the two double bonds over both hydrocarbon tails, we also considered C(16:0)–C(18:2)PC (palmitoyl-linoleoyl-PC, PLiPC) as the unsaturated component. In PLiPC, both double bonds are located in the *sn-2* tail, while the *sn-1* tail is completely saturated. In previous simulations of a DPPC/DLiPC/cholesterol bilayer doped with 2 mol-% PLiPC, the hybrid saturated/unsaturated tail lipid was found to co-localize with the DLiPC lipids in the l_d domain [49], suggesting that PLiPC might also form a stable l_d domain on its own. Fig. 3 (panels G–I) shows that the DPPC/PLiPC/cholesterol mixture does not phase separate during our simulation. The RDFs reveal that the mixing is not ideal on a length-scale extending up to about 2.5 nm. The partitioning

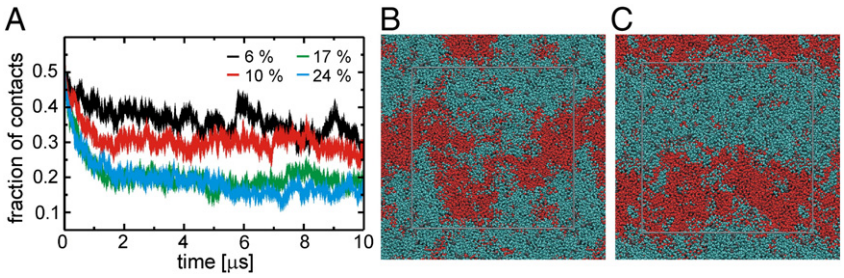

Fig. 4. Effect of cholesterol concentration on lipid mixing in ternary DPPC/DLiPC/cholesterol bilayers. A) Fraction of contacts between DLiPC and DPPC lipids. B, C) Final snapshots from CG–MD simulations with 6 (B) and 10 mol-% (C) cholesterol.

behavior of DPPC/PLiPC/cholesterol mixtures still remains to be characterized experimentally.

To further quantify the degree of non-ideal mixing, we calculated the preferential solvation parameters, δ, from the Kirkwood–Buff integrals (see Section 2.4.3). For ideal mixtures, $\delta = 0$, whereas $\delta > 0$ indicates non-ideal mixing. The preferential solvation parameters found for the ternary DDPC/DLiPC/cholesterol, DPPC/DOPC/cholesterol, and DPPC/PLiPC/cholesterol systems are $\delta = 0.8$, $\delta = 1.1$, and $\delta = 1.8$, respectively. Thus, of these three mixtures, the PLiPC-containing bilayer deviates most strongly from ideal mixing.

3.2. Cholesterol is essential for complete fluid/fluid phase separation

Cholesterol plays a crucial role for phase separation into coexisting fluid domains. Binary mixtures of DOPC and saturated PC lipids do not show liquid/liquid coexistence [16] at any temperature, although at low temperatures, liquid/gel segregation can occur. Addition of at least ~10 mol-% cholesterol, however, can trigger the segregation into μm-sized l_o and l_d fluid domains [16,19]. We systematically investigated the effect of cholesterol on the mixing behavior of ternary DPPC/DLiPC/cholesterol bilayers by varying its concentration in the range 6–30 mol-%. Fig. 4 shows that phase separation into two distinct lipid domains was observed at all cholesterol concentrations investigated. The segregation of the systems with 6 and 10 mol-% was significantly slower than for the higher cholesterol concentrations (Fig. 4A), indicating a reduced driving force for demixing. As shown in Table 1, the line tension drops approximately linearly in the 17–30 mol-% concentration range, with the 10 and 6 mol-% cholesterol mixtures having line tensions of ~1–2 pN. Consistent with the low line tensions, the domains formed in these simulations were highly dynamic on the time- and length-scales of our simulations, with a strongly fluctuating boundary interface (Fig. 4B, C).

In this context, it is also interesting to investigate the effect of completely removing cholesterol, i.e., a binary DPPC/DLiPC mixture. Based on the experimental results obtained for DOPC as the unsaturated component [16,19], it may be expected that macroscopic phase separation should not occur in the simulations. Indeed, in previous CG-MARTINI simulations of binary DPPC/DLiPC mixtures, no segregation was observed at 295 K, although the mixing of the two lipid components was not ideal, with density fluctuations on the nm length scale [44,70]. Compared to DOPC, the doubly unsaturated DLiPC used in our simulations increases the tendency to demix, explaining the low concentration of cholesterol sufficient for phase separation (<6 mol-% in the case of DLiPC, compared to >10 mol-% for DOPC [16,19]).

3.3. TM helices accumulate in l_d phase and amplify non-ideal mixing close to the critical point

To probe the influence of TM helices on the phase separation of the lipids, we inserted 64 α-helical WALP23 peptides into the ternary DPPC/DLiPC/cholesterol and DPPC/PLiPC/cholesterol bilayers, respectively, yielding simulation systems with a peptide-to-lipid ratio of ~23% by mass (Table 1). This high concentration of TM helices was chosen to mimic the highly crowded situation in some biological membranes, which can contain up to 50–75 mass-% of proteins (this fraction also includes the non-TM parts of the proteins) [29]. We used WALP peptides as canonical models for α-helical TM domains (Fig. 1). WALPs are comprised of alternating alanine and leucine residues, flanked by tryptophanes to anchor the peptide in the membrane interface. They were designed as probes to study the behavior of TM domains in model systems, such as their mode of insertion, aggregation, and partitioning [71]. In our previous simulation study [48], we found that WALP peptides have a strong thermodynamic preference for the l_d phase: the free energy difference of transferring a single monomeric WALP23 from l_o to l_d is about -60 kJ mol^{-1} in the segregated DPPC/DLiPC/cholesterol bilayer. Furthermore, from counting the number of dimers observed during the simulations [72], we predicted a dimerization free energy of -12 ± 2 kJ mol^{-1} for WALP23 in the DLiPC-containing l_d domain [48], in agreement with fluorescence resonance energy transfer (FRET) experiments on similar model TM α-helices [73]. Thus, both the l_o/l_d partitioning and the interactions (dimerization) of the TM helices are realistically described by the MARTINI CG model, motivating our choice for the WALP peptides.

3.3.1. Quaternary DPPC/DLiPC/cholesterol/WALP23 system

Here we consider the effect of the TM peptides on the strongly phase-separating DPPC/DLiPC/cholesterol mixture. Fig. 5 shows that phase separation occurs even in the presence of a high concentration of TM helices; similar results were obtained in additional simulations with a peptide-to-lipid (P/L) ratio of 35 mass-% (not shown). Judged by the fraction of lipid–lipid contacts (Fig. 5B), phase separation is completed after about 5 μs, similar to the simulation without peptides. All WALP23 peptides segregate into the l_d domain, in agreement with the strong thermodynamic preference for l_d. The segregation of the TM helices into the disordered domain leads to a very high P/L ratio of about

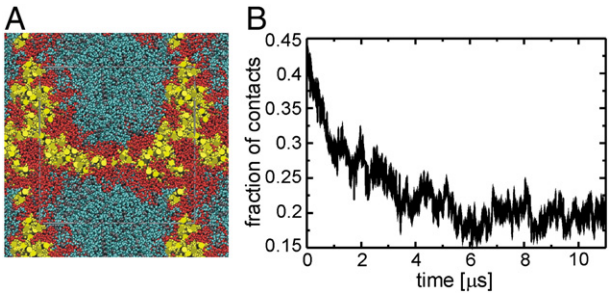

Fig. 5. DPPC/DLiPC/cholesterol bilayer containing 64 α-helical WALP23 TM peptides (P/L = 1:5 in l_d). A) Snapshot after 11 μs of CG–MD simulation. DPPC is colored cyan, DLiPC red, cholesterol gray, WALP23 is shown as yellow cylinders. B) Fraction of DLiPC–DPPC contacts.

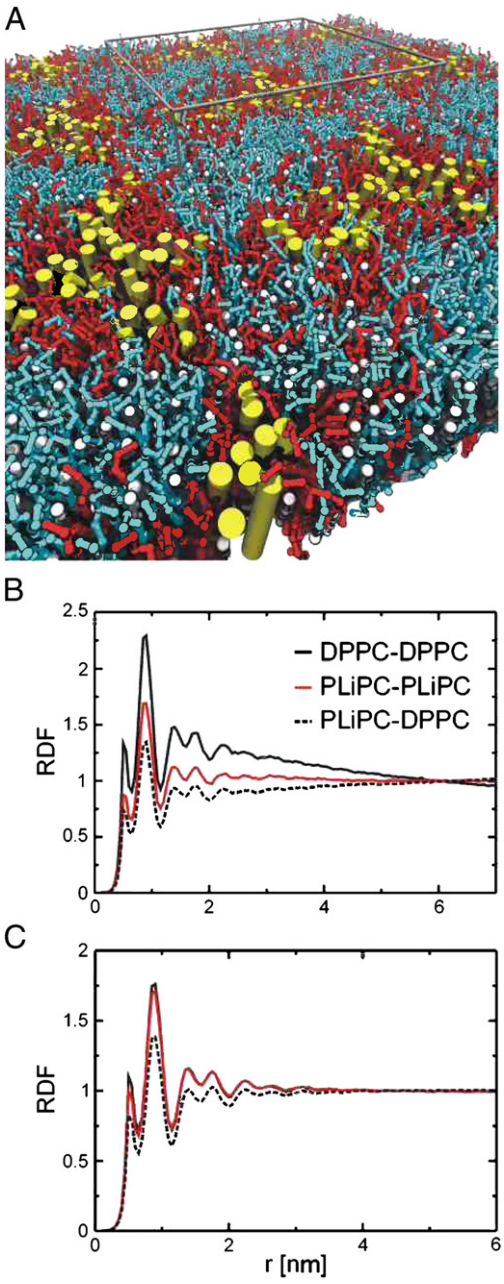

Fig. 6. DPPC/PLiPC/cholesterol bilayer containing WALP23 TM peptides. A) Snapshot after 12 μs from CG–MD simulation of bilayer containing 64 WALP23 peptides (color code the same as in Fig. 5). The periodic simulation box is shown in gray. B, C) Radial distribution functions of lipids in bilayers with 64 (B) and 12 (C) WALP23 peptides.

1:5 in l_d. As a consequence, almost all WALPs are loosely connected and form one large network.

3.3.2. Quaternary DPPC/PLiPC/cholesterol/WALP23 system

Next, we investigated how TM helices alter the phase behavior of the ternary DPPC/PLiPC/cholesterol mixture. In the absence of TM helices, this bilayer did not segregate into two distinct lipid phases in our simulation at 295 K, although the mixing is not ideal up to a length scale of ~2.5 nm (Fig. 3). Fig. 6 shows that in the presence of a high concentration of WALP23 TM peptides, the lipids are more heterogeneously mixed. The RDFs in Fig. 6B display long-range tails that cross at around 6 nm, indicating differential solvation of the lipid components up to this length scale. The amplification of non-ideal lipid mixing is also evident from evaluation of the Kirkwood–Buff integrals (up to $R_c = 6$ nm), which yielded a preferential solvation parameter of $\delta = 15.1$, as compared to $\delta = 1.8$ in the system without TM helices (Section 3.1.4). The WALP TM helices bind unsaturated lipids preferably over saturated ones and cholesterol. Since the DPPC/PLiPC/cholesterol mixture is relatively close to the critical point, the free energy penalty for demixing of the lipid components is rather small. By bridging the unsaturated lipids, the weak (lipid-mediated) connectivity between the TM peptides thus couples to the level of the lipids as well, promoting their segregation. This interpretation implies that the size of the formed lipid domains should depend on the concentration of TM peptides. To test this hypothesis, we carried out an additional 20-μs CG–MD simulation with only 12 WALP23 TM peptides in the DPPC/PLiPC/cholesterol bilayer (Table 1). The RDFs in Fig. 6C show that, indeed, this lower concentration has a much less pronounced effect. The WALP TM peptides form small and transient clusters (mostly dimers, trimers, and tetramers), which occasionally exchange individual monomers between them through dissociation/reassociation (not shown), qualitatively similar to our previous simulations [48]. The preferential solvation of these small clusters by unsaturated lipids is not sufficient to induce non-ideal lipid mixing on a length scale >3.5 nm.

3.4. Crowding slows down lateral diffusion

The clustering of the TM helices is a slow process. The mean square displacement (MSD) curves (see Section 2.4) in Fig. 7 show that the WALP peptides in the highly crowded l_d domain of the DPPC/DLiPC/cholesterol bilayer (Fig. 5) need about 0.4 μs to sample a root mean square distance of ~1 nm in the membrane plane, which corresponds roughly to their own diameter. Thus, although several transient binding/unbinding events of individual monomers are observed, our simulation is clearly not long enough to achieve full sampling; the required ms time scale is currently out of reach even for our CG–MD approach. The MSD of the 64 WALP peptides in the crowded bilayer (Fig. 7, black squares) may be compared to the more dilute case of only 12 WALP23 peptides (P/L = 1:50, black crosses). These latter data were extracted from our previous simulation [48], in which the peptides were observed to form small transient clusters, mostly dimers. Since the l_d phase comprised of 540 DLiPC lipids in our previous simulation [48], the P/L ratio was about 1:50, compared to 1:5 in the l_d phase of the crowded bilayer. The MSD curves in Fig. 7 show that the lateral diffusion of the TM peptides in the crowded system is slowed down by a factor of ~10 in the long-time limit as compared to the more dilute bilayer, in agreement with experimental findings [74–77]. In addition to the TM peptides, also the diffusivity of the lipids is affected: the motion of the DLiPC lipids in the l_d domain is confined by the TM helices, slowing down diffusion by about a factor of 5 in the long-time limit as compared to the more dilute case (red curves in Fig. 7). These results agree

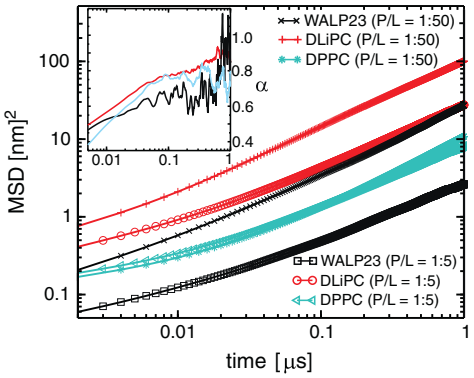

Fig. 7. Mean square displacements (MSD) of lipids and TM helices in CG–MD simulations with 64 (P/L ratio 1:5 in l_d) and 12 TM helices (P/L ratio 1:50 in l_d), respectively, in the phase-separated DPPC/DLiPC/cholesterol bilayer. Inset: Anomaly exponents, α, from simulation with 64 TM helices. The small copy number of TM helices and slow lateral motions limit the sampling at long time scales.

with a recent all-atom MD simulation study of a voltage-gated ion channel in a lipid bilayer [78], which showed that lipids within a radius of ~3 nm from the protein surface diffuse significantly slower than bulk lipids. In our simulation, there are essentially no bulk ("free") lipids in the highly crowded l_d domain, because they are either bound to the TM helices or close to the domain boundary interface. By contrast, the diffusivity of the DPPC lipids in the peptide-free l_o domain was not significantly slowed down (cyan curves in Fig. 7).

Different possible reasons for the observed retardation of diffusion in cellular environments were suggested, emphasizing the role of cortical factors, such as actin or spectrin filaments (pickets and fences model, [75]), or an increased apparent membrane viscosity due to molecular crowding [76,77,79]. Our findings seem to support the crowding model, as we observe a significant slowing down in the absence of a cytoskeleton. However, this interpretation has to be taken with care, because of the different length- and time scales covered by our simulations (~10 nm, μs) and typical experiments, such as single-molecule tracking (~100 nm, ms). In fact, a transient scaling of the apparent diffusion coefficient in biological membranes over several orders of magnitude is observed [74,75,80–83]. Such anomalous diffusion, or subdiffusion, is characterized by a nonlinear dependence of the MSD on time, i.e., MSD $\sim t^{\alpha}$ with $\alpha<1$. Several microscopic models for subdiffusion have been suggested, such as obstruction [82], fractional Brownian motion [84], and the continuous-time random walk [85]. Owing to the complex composition of cellular membranes, it is still discussed whether these models can explain the actual physical origin of subdiffusion [86–88]. The current interest in subdiffusion as an efficient mechanism of search and association in physiological situations [89,90] motivated recent molecular simulation studies, which provided detailed insights into subdiffusive behavior of lipids [91] and linear polymers of model TM proteins [92] in bilayers. Fig. 7 (inset) shows the anomaly exponent, α, as obtained from our simulation with 64 TM helices, i.e., with P/L = 1:5 in l_d. Subdiffusive behavior ($\alpha<1$) occurs up to the μs observation time, since the motion of the molecules is confined to the respective domains on this time scale. For longer observation times, the diffusion will slowly but unequivocally approach the normal Brownian regime characterized by $\alpha = 1$.

3.5. Bacteriorhodopsin partitions into l_d domains

Finally, instead of using individual TM α-helices, we studied the l_o/l_d partitioning of the α-helical 7-TM protein bacteriorhodopsin (bR). In giant unilamellar vesicles composed of a 1:1:1 mixture of sphingomyelin, DOPC, and cholesterol, bR was found to partition into the l_d domains with a partition coefficient of ~50 at a protein-to-lipid molar ratio of about 1:1000 [93]. In our simulation of a single bR molecule embedded in the phase-separating DPPC/DLiPC/cholesterol bilayer, we found bR to partition into the l_d domain, in agreement with experiment. The headgroup-headgroup distance is 4.6 and 3.65 nm in the l_o and l_d domains, respectively (Fig. 2), implying hydrophobic thicknesses of about 3.6 and 2.65 nm, respectively. Since the TM dimension of the hydrophobic surface of bR is ~3.0 nm [94], the observed partitioning of the protein into l_d could be expected simply based on hydrophobic matching. To test this, we set up a second simulation with DMPC instead of DPPC, which reduces the hydrophobic thickness of the l_o domain to ~2.9 nm (Fig. 2). Thus, in this latter bilayer, bR fits better (in terms of hydrophobic matching) into the l_o than into the l_d domain. As shown in Fig. 8, also in this simulation, bR partitions into the l_d domain. These results provide further support for the experimental finding that hydrophobic matching alone does not determine the l_o/l_d partitioning of TM proteins in synthetic model membranes [95–102], since the enthalpically unfavorable disturbance of the tight packing of the lipids in the l_o domains drives the TM inclusions into the l_d domains [48]. Although the situation in model membranes differs from that in real cell membranes, it may thus not be surprising that post-translational lipidation is an important and often required additional factor for raft targeting of TM proteins [103,104].

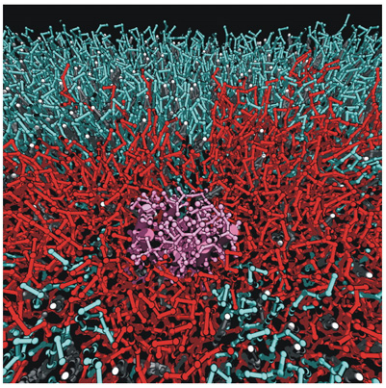

Fig. 8. Bacteriorhodopsin (purple) prefers the l_d (red) over the l_o domain (cyan).

We are currently investigating the partitioning of lipid-anchored proteins with CG–MD simulations.

4. Conclusions

In this work, we studied heterogeneous multi-component mixtures of saturated lipids, unsaturated lipids, cholesterol, and TM proteins using coarse-grained molecular dynamics simulations. We showed that reducing the mismatch between the length of the saturated and unsaturated lipid tails leads to a smaller driving force for segregation into coexisting liquid-ordered and -disordered lipid domains. Furthermore, we quantified the effect of cholesterol, which is essential for phase separation. For the DPPC/DLiPC/cholesterol lipid mixture, which has a strong tendency to segregate, macroscopic phase separation was found also in the presence of a high concentration of α-helical transmembrane peptides that partitioned into the liquid-disordered domain. The crowding in the formed lipid/TM helix domain, which may be reminiscent of biological membranes, significantly slowed down lateral diffusion by a factor 5–10 as compared to the dilute case. Furthermore, simulations of the DPPC/PLiPC/cholesterol bilayer, which in the absence of TM α-helices less strongly deviated from ideal mixing behavior, showed that a sufficiently high concentration of TM peptides can enhance the non-ideal mixing of the lipids and bring the system close to the miscibility critical point. Finally, the 7-TM protein bacteriorhodopsin was found to partition into the liquid-disordered domains in phase-separated bilayers, irrespective of hydrophobic matching.

The current quantitative proteomics/lipidomics and structural genomics approaches continue to map out the molecular structures and compositions of organisms with ever increasing detail. A challenge is to use this information to construct realistic in silico models, which can provide deep insights into the collective behavior of individual molecules that leads to the complex structural organization found in biological membranes. In this context, our work shows that it is possible to directly simulate the dynamic interplay and reorganization of lipids and proteins in compositionally heterogeneous and crowded model biomembranes with efficient yet chemically detailed coarse-grained models, a step toward realistic simulations of simple yet compositionally complete cellular membranes.

Acknowledgements

We thank M. Deserno for useful discussions and G. Feigenson and P. Tieleman for carefully reading the manuscript prior to publication. Support from the Netherlands Organisation for Scientific Research (NWO) is thankfully acknowledged (Veni grant 700.57.404 to LVS,

CW-Top grant 700.57.303 to SJM). JD was supported by the ERASMUS program.

References

[1] S.J. Singer, G.L. Nicholson, The fluid mosaic model of the structure of cell membranes, Science 175 (1972) 720–731.
[2] K. Simons, E. Ikonen, Functional rafts in cell membranes, Nature 387 (1997) 569–572.
[3] J.U. Bowie, Solving the membrane protein folding problem, Nature 438 (2005) 581–589.
[4] D.M. Engelman, Membranes are more mosaic than fluid, Nature 438 (2005) 578–580.
[5] L.H. Chamberlain, R.D. Burgoyne, G.W. Gould, SNARE proteins are highly enriched in lipid rafts in PC12 cells: implications for the spatial control of exocytosis, Proc. Natl. Acad. Sci. U. S. A. 98 (2001) 5619–5624.
[6] T. Lang, D. Bruns, D. Wenzel, D. Riedel, P. Holroyd, C. Thiele, R. Jahn, SNAREs are concentrated in cholesterol-dependent clusters that define docking and fusion sites for exocytosis, EMBO J. 20 (2001) 2202–2213.
[7] M.S. Bretscher, S. Munro, Cholesterol and the Golgi apparatus, Science 261 (1993) 1280–1281.
[8] M. Kawabuchi, Y. Satomi, T. Takao, Y. Shimonishi, S. Nada, K. Nagai, A. Tarakhovsky, M. Okada, Transmembrane phosphoprotein Cbp regulates the activities of Src-family tyrosine kinases, Nature 404 (2000) 999–1003.
[9] S. Moffett, D.A. Brown, M.E. Linder, Lipid-dependent targeting of G proteins into rafts, J. Biol. Chem. 275 (2000) 2191–2198.
[10] K. Simons, D. Toomre, Lipid rafts and signal transduction, Nat. Rev. Mol. Cell Biol. 1 (2000) 31–39.
[11] C. Eggeling, C. Ringemann, R. Medda, G. Schwarzmann, K. Sandhoff, S. Polyakova, V.N. Belov, B. Hein, C. von Middendorff, A. Schonle, S.W. Hell, Direct observation of the nanoscale dynamics of membrane lipids in a living cell, Nature 457 (2009) 1159–1162.
[12] J.F. Hancock, Lipid rafts: contentious only from simplistic standpoints, Nat. Rev. Mol. Cell Biol. 7 (2006) 456–462.
[13] M. Edidin, The state of lipid rafts: from model membranes to cells, Annu. Rev. Biophys. Biomol. Struct. 32 (2003) 257–283.
[14] K. Jacobson, O.G. Mouritsen, R.G.W. Anderson, Lipid rafts: at a crossroad between cell biology and physics, Nat. Cell Biol. 9 (2007) 7–14.
[15] A.V. Samsonov, I. Mihalyov, F.S. Cohen, Characterization of cholesterol–sphingomyelin domains and their dynamics in bilayer membranes, Biophys. J. 81 (2001) 1486–1500.
[16] S.L. Veatch, S.L. Keller, Organization in lipid membranes containing cholesterol, Phys. Rev. Lett. 89 (2002) 268101.
[17] T. Baumgart, S.T. Hess, W.W. Webb, Imaging coexisting fluid domains in biomembrane models coupling curvature and line tension, Nature 425 (2003) 821–824.
[18] N. Kahya, D. Scherfeld, K. Bacia, B. Poolman, P. Schwille, Probing lipid mobility of raft-exhibiting model membranes by fluorescence correlation spectroscopy, J. Biol. Chem. 278 (2003) 28109–28115.
[19] S.L. Veatch, S.L. Keller, Separation of liquid phases in giant vesicles of ternary mixtures of phospholipids and cholesterol, Biophys. J. 85 (2003) 3074–3083.
[20] H.-J. Kaiser, D. Lingwood, I. Levental, J.L. Sampaio, L. Kalvodova, L. Rajendran, K. Simons, Order of lipid phases in model and plasma membranes, Proc. Natl. Acad. Sci. U. S. A. 106 (2009) 16645–16650.
[21] D. Lingwood, J. Ries, P. Schwille, K. Simons, Plasma membranes are poised for activation of raft phase coalescence at physiological temperature, Proc. Natl. Acad. Sci. U. S. A. 105 (2008) 10005–10010.
[22] T. Baumgart, A.T. Hammond, P. Sengupta, S.T. Hess, D.A. Holowka, B.A. Baird, W.W. Webb, Large-scale fluid/fluid phase separation of proteins and lipids in giant plasma membrane vesicles, Proc. Natl. Acad. Sci. U. S. A. 104 (2007) 3165–3170.
[23] S. Munro, Lipid rafts: elusive or illusive? Cell 115 (2003) 377–388.
[24] G.W. Feigenson, Phase boundaries and biological membranes, Annu. Rev. Biophys. Biomol. Struct. 36 (2007) 63–77.
[25] E. London, How principles of domain formation in model membranes may explain ambiguities concerning lipid raft formation in cells, Biochim. Biophys. Acta 1746 (2005) 203–220.
[26] S.L. Veatch, P. Cicuta, P. Sengupta, A. Honerkamp-Smith, D. Holowka, B. Baird, Critical fluctuations in plasma membrane vesicles, ACS Chem. Biol. 3 (2008) 287–293.
[27] G. van Meer, D.R. Voelker, G.W. Feigenson, Membrane lipids: where they are and how they behave, Nat. Rev. Mol. Cell Biol. 9 (2008) 112–124.
[28] T.A. Ryan, J. Myers, D. Holowka, B. Baird, W.W. Webb, Molecular crowding on the cell surface, Science 239 (1988) 61–64.
[29] G. Guidotti, Membrane proteins, Annu. Rev. Biochem. 41 (1972) 731–752.
[30] R.G.W. Anderson, K. Jacobson, Cell biology — a role for lipid shells in targeting proteins to caveolae, rafts, and other lipid domains, Science 296 (2002) 1821–1825.
[31] D. Lingwood, K. Simons, Lipid rafts as a membrane-organizing principle, Science 327 (2010) 46–50.
[32] W. Helfrich, Elastic properties of lipid bilayers—theory and possible experiments, Z. Naturforsch. C 28 (1973) 693–703.
[33] O.G. Mouritsen, M. Bloom, Mattress model of lipid–protein interactions in membranes, Biophys. J. 46 (1984) 141–153.
[34] S.J. Marrink, A.H. de Vries, D.P. Tieleman, Lipids on the move: simulations of membrane pores, domains, stalks and curves, BBA Biomembr. 1788 (2009) 149–168.
[35] G.A. Voth, Coarse-Graining of Condensed Phase and Biomolecular Systems, CRC Press/ Taylor and Francis, Boca Raton, FL, 2009.
[36] E. Psachoulia, D.P. Marshall, M.S.P. Sansom, Molecular dynamics simulations of the dimerization of transmembrane alpha-helices, Acc. Chem. Res. 43 (2010) 388–396.
[37] X. Periole, T. Huber, S.J. Marrink, T.P. Sakmar, G protein-coupled receptors self-assemble in dynamics simulations of model bilayers, J. Am. Chem. Soc. 129 (2007) 10126–10132.
[38] U. Schmidt, G. Guigas, M. Weiss, Cluster formation of transmembrane proteins due to hydrophobic mismatching, Phys. Rev. Lett. 101 (2008) 128104.
[39] B.J. Reynwar, M. Deserno, Membrane composition-mediated protein–protein interactions, Biointerphases 3 (2008) FA117–FA124.
[40] F.J.-M. de Meyer, M. Venturoli, B. Smit, Molecular simulations of lipid-mediated protein–protein interactions, Biophys. J. 95 (2008) 1851–1865.
[41] D. Sengupta, S.J. Marrink, Lipid-mediated interactions tune the association of glycophorin A helix and its disruptive mutants in membranes, Phys. Chem. Chem. Phys. 12 (2010) 12987–12996.
[42] D. Morozova, G. Guigas, M. Weiss, Dynamic structure formation of peripheral membrane proteins, PLoS Comput. Biol. 7 (2011) e1002067.
[43] B. West, F.L.H. Brown, F. Schmid, Membrane–protein interactions in a generic coarse-grained model for lipid bilayers, Biophys. J. 96 (2009) 101–115.
[44] H.J. Risselada, S.J. Marrink, The molecular face of lipid rafts in model membranes, Proc. Natl. Acad. Sci. U. S. A. 105 (2008) 17367–17372.
[45] S.J. Marrink, H.J. Risselada, S. Yefimov, D.P. Tieleman, A.H. de Vries, The MARTINI force field: coarse grained model for biomolecular simulations, J. Phys. Chem. B 111 (2007) 7812–7824.
[46] L. Monticelli, S.K. Kandasamy, X. Periole, R.G. Larson, D.P. Tieleman, S.J. Marrink, The MARTINI coarse-grained force field: extension to proteins, J. Chem. Theory Comput. 4 (2008) 819–834.
[47] S.L. Veatch, I.V. Polozov, K. Gawrisch, S.L. Keller, Liquid domains in vesicles investigated by NMR and fluorescence microscopy, Biophys. J. 86 (2004) 2910–2922.
[48] L.V. Schäfer, D.H. de Jong, A. Holt, A.J. Rzepiela, A.H. de Vries, B. Poolman, J.A. Killian, S.J. Marrink, Lipid packing drives the segregation of transmembrane helices into disordered lipid domains in model membranes, Proc. Natl. Acad. Sci. U. S. A. 108 (2011) 1343–1348.
[49] L.V. Schäfer, S.J. Marrink, Partitioning of lipids at domain boundaries in model membranes, Biophys. J. 99 (2010) L91–L93.
[50] A. Tian, C. Johnson, W. Wang, T. Baumgart, Line tension at fluid membrane domain boundaries measured by micropipette aspiration, Phys. Rev. Lett. 98 (2007) 208102.
[51] B. Hess, C. Kutzner, D. van der Spoel, E. Lindahl, GROMACS 4: algorithms for highly efficient, load-balanced, and scalable molecular simulation, J. Chem. Theory Comput. 4 (2008) 435–447.
[52] S.J. Marrink, H.J. Risselada, A.E. Mark, Simulation of gel phase formation and melting in lipid bilayers using a coarse grained model, Chem. Phys. Lipids 135 (2005) 223–244.
[53] T. Schneider, E. Stoll, Molecular-dynamics study of a three-dimensional one-component model for distortive phase transitions, Phys. Rev. B 17 (1978) 1302–1322.
[54] G. Bussi, M. Parrinello, Stochastic thermostats: comparison of local and global schemes, Comput. Phys. Commun. 179 (2008) 26–29.
[55] G. Bussi, D. Donadio, M. Parrinello, Canonical sampling through stochastic velocity-rescaling, J. Chem. Phys. 126 (2007) 014101.
[56] S.E. Feller, K. Gawrisch, A.D. MacKerell, Polyunsaturated fatty acids in lipid bilayers: intrinsic and environmental contributions to their unique physical properties, J. Am. Chem. Soc. 124 (2002) 318–326.
[57] S.J. Marrink, A.H. de Vries, T.A. Harroun, J. Katsaras, S.R. Wassall, Cholesterol shows preference for the interior of polyunsaturated lipid membranes, J. Am. Chem. Soc. 130 (2008) 10–11.
[58] N. Kucerka, D. Marquardt, T.A. Harroun, M.-P. Nieh, S.R. Wassall, D.H.d. Jong, L.V. Schäfer, S.J. Marrink, J. Katsaras, Cholesterol in bilayers with PUFA chains: doping with DMPC or POPC results in sterol reorientation and membrane-domain formation, Biochemistry 49 (2010) 7485–7493.
[59] T. Apajalahti, P. Niemelä, P.N. Govindan, M. Miettinen, E.E. Salonen, S.J. Marrink, I. Vattulainen, Concerted diffusion of lipids in raft-like membranes, Faraday Discuss. 144 (2010) 411–430.
[60] J.D. Perlmutter, J.N. Sachs, Interleaflet interaction and asymmetry in phase separated lipid bilayers: molecular dynamics simulations, J. Am. Chem. Soc. 133 (2011) 6563–6577.
[61] H. Luecke, B. Schobert, H.T. Richter, J.P. Cartailler, J.K. Lanyi, Structure of bacteriorhodopsin at 1.55 A resolution, J. Mol. Biol. 291 (1999) 899–911.
[62] W. Kabsch, C. Sander, Dictionary of protein secondary structure: pattern recognition of hydrogen-bonded and geometrical features, Biopolymers 22 (1983) 2577–2637.
[63] X. Periole, M. Cavalli, S.J. Marrink, M. Ceruso, Combining an elastic network with a coarse-grained molecular force field: structure, dynamics and intermolecular recognition, J. Chem. Theory Comput. 5 (2009) 2531–2543.
[64] B. Hess, Determining the shear viscosity of model liquids from molecular dynamics simulations, J. Chem. Phys. 116 (2002) 209–217.
[65] J.G. Kirkwood, F.P. Buff, The statistical mechanical theory of solutions, J. Chem. Phys. 19 (1951) 774–779.
[66] S. Ramadurai, A. Holt, L.V. Schäfer, V.V. Krasnikov, D.T.S. Rijkers, S.J. Marrink, J.A. Killian, B. Poolman, Influence of hydrophobic mismatch and amino acid composition on the lateral diffusion of transmembrane peptides, Biophys. J. 99 (2010) 1447–1454.

[67] D. Fritz, K. Koschke, V.A. Harmandaris, N.F.A. van der Vegt, K. Kremer, Multiscale modeling of soft matter: scaling of dynamics, Phys. Chem. Chem. Phys. 13 (2011) 10412–10420.
[68] T.P.W. McMullen, R.N. McElhaney, Physical studies of cholesterol–phospholipid interactions, Curr. Opin. Colloid Interface Sci. 1 (1996) 83–90.
[69] S.A. Akimov, P.I. Kuzmin, J. Zimmerberg, F.S. Cohen, Y.A. Chizmadzhev, An elastic theory for line tension at a boundary separating two lipid monolayer regions of different thickness, J. Electroanal. Chem. 564 (2004) 13–18.
[70] C. Rosetti, C. Pastorino, Polyunsaturated and saturated phospholipids in mixed bilayers: a study from the molecular scale to the lateral lipid organization, J. Phys. Chem. B 115 (2010) 1002–1013.
[71] T.K.M. Nyholm, S. Özdirekcan, J.A. Killian, How protein transmembrane segments sense the lipid environment, Biochemistry 46 (2007) 1457–1465.
[72] D.H. de Jong, L.V. Schäfer, A.H. de Vries, S.J. Marrink, H.J.C. Berendsen, H. Grubmüller, Determining equilibrium constants for dimerization reactions from molecular dynamics simulations, J. Comput. Chem. 32 (2011) 1919–1928.
[73] Y. Yano, K. Matsuzaki, Measurement of thermodynamic parameters for hydrophobic mismatch 1: self-association of a transmembrane helix, Biochemistry 45 (2006) 3370–3378.
[74] M.J. Saxton, K. Jacobson, Single-particle tracking: applications to membrane dynamics, Annu. Rev. Biophys. Biomol. Struct. 26 (1997) 373–399.
[75] A. Kusumi, C. Nakada, K. Ritchie, K. Murase, K. Suzuki, H. Murakoshi, R.S. Kasai, J. Kondo, T. Fujiwara, Paradigm shift of the plasma membrane concept from the two-dimensional continuum fluid to the partitioned fluid: high-speed single-molecule tracking of membrane molecules, Annu. Rev. Biophys. Biomol. Struct. 34 (2005) 351–378.
[76] M. Frick, K. Schmidt, B.J. Nichols, Modulation of lateral diffusion in the plasma membrane by protein density, Curr. Biol. 17 (2007) 462–467.
[77] D.F. Kucik, E.L. Elson, M.P. Sheetz, Weak dependence of mobility of membrane protein aggregates on aggregate size supports a viscous model of retardation of diffusion, Biophys. J. 76 (1999) 314–322.
[78] P.S. Niemelä, M.S. Miettinen, L. Monticelli, H. Hammaren, P. Bjelkmar, T. Murtola, E. Lindahl, I. Vattulainen, Membrane proteins diffuse as dynamic complexes with lipids, J. Am. Chem. Soc. 132 (2010) 7574–7575.
[79] M.P. Sheetz, Glycoprotein motility and dynamic domains in fluid plasma membranes, Annu. Rev. Biophys. Biomol. Struct. 22 (1993) 417–431.
[80] M. Weiss, H. Hashimoto, T. Nilsson, Anomalous protein diffusion in living cells as seen by fluorescence correlation spectroscopy, Biophys. J. 84 (2003) 4043–4052.
[81] K. Ritchie, X.Y. Shan, J. Kondo, K. Iwasawa, T. Fujiwara, A. Kusumi, Detection of non-Brownian diffusion in the cell membrane in single molecule tracking, Biophys. J. 88 (2005) 2266–2277.
[82] M.J. Saxton, Anomalous diffusion due to obstacles: a Monte Carlo study, Biophys. J. 66 (1994) 394–401.
[83] T.J. Feder, I. Brust-Mascher, J.P. Slattery, B. Baird, W.W. Webb, Constrained diffusion or immobile fraction on cell surfaces: a new interpretation, Biophys. J. 70 (1996) 2767–2773.
[84] M.J. Saxton, Anomalous subdiffusion in fluorescence photobleaching recovery: a Monte Carlo study, Biophys. J. 81 (2001) 2226–2240.
[85] R. Metzler, J. Klafter, The random walk's guide to anomalous diffusion: a fractional dynamics approach, Phys. Rep. 339 (2000) 1–77.
[86] J. Szymanski, M. Weiss, Elucidating the origin of anomalous diffusion in crowded fluids, Phys. Rev. Lett. 103 (2009) 038102.
[87] M. Magdziarz, A. Weron, K. Burnecki, J. Klafter, Fractional Brownian motion versus the continuous-time random walk: a simple test for subdiffusive dynamics, Phys. Rev. Lett. 103 (2009) 180602.
[88] V. Tejedor, O. Bénichou, R. Voituriez, R. Jungmann, F. Simmel, C. Selhuber-Unkel, L.B. Oddershede, R. Metzler, Quantitative analysis of single particle trajectories: mean maximal excursion method, Biophys. J. 98 (2010) 1364–1372.
[89] G. Guigas, M. Weiss, Sampling the cell with anomalous diffusion — the discovery of slowness, Biophys. J. 94 (2008) 90–94.
[90] I. Golding, E.C. Cox, Physical nature of bacterial cytoplasm, Phys. Rev. Lett. 96 (2006) 098102.
[91] E. Flenner, J. Das, M.C. Rheinstädter, I. Kosztin, Subdiffusion and lateral diffusion coefficient of lipid atoms and molecules in phospholipid bilayers, Phys. Rev. E 79 (2009) 011907.
[92] U. Schmidt, M. Weiss, Anomalous diffusion of oligomerized transmembrane proteins, J. Chem. Phys. 134 (2011) 165101.
[93] N. Kahya, D.A. Brown, P. Schwille, Raft partitioning and dynamic behavior of human placental alkaline phosphatase in giant unilamellar vesicles, Biochemistry 44 (2005) 7479–7489.
[94] B.A. Lewis, D.M. Engelman, Bacteriorhodopsin remains dispersed in fluid phospholipid bilayers over a wide range of bilayer thicknesses, J. Mol. Biol. 166 (1983) 203–210.
[95] H. Shogomori, A.T. Hammond, A.G. Ostermeyer-Fay, D.J. Barr, G.W. Feigenson, E. London, D.A. Brown, Palmitoylation and intracellular domain interactions both contribute to raft targeting of linker for activation of T cells, J. Biol. Chem. 280 (2005) 18931–18942.
[96] T.J. McIntosh, A. Vidal, S.A. Simon, Sorting of lipids and transmembrane peptides between detergent-soluble bilayers and detergent-resistant rafts, Biophys. J. 85 (2003) 1656–1666.
[97] J. Nikolaus, S. Scolari, E. Bayraktarov, N. Jungnick, S. Engel, A.P. Plazzo, M. Stöckl, R. Volkmer, M. Veit, A. Herrmann, Hemagglutinin of influenza virus partitions into the nonraft domain of model membranes, Biophys. J. 99 (2010) 489–498.
[98] M.E. Fastenberg, H. Shogomori, X. Xu, D.A. Brown, E. London, Exclusion of a transmembrane-type peptide from ordered-lipid domains (rafts) detected by fluorescence quenching: extension of quenching analysis to account for the effects of domain size and domain boundaries, Biochemistry 42 (2003) 12376–12390.
[99] A. Vidal, T.J. McIntosh, Transbilayer peptide sorting between raft and nonraft bilayers: comparisons of detergent extraction and confocal microscopy, Biophys. J. 89 (2005) 1102–1108.
[100] K. Bacia, C.G. Schuette, N. Kahya, R. Jahn, P. Schwille, SNAREs prefer liquid-disordered over "raft" (liquid-ordered) domains when reconstituted into giant unilamellar vesicles, J. Biol. Chem. 279 (2004) 37951–37955.
[101] A.T. Hammond, F.A. Heberle, T. Baumgart, D. Holowka, B. Baird, G.W. Feigenson, Crosslinking a lipid raft component triggers liquid ordered–liquid disordered phase separation in model plasma membranes, Proc. Natl. Acad. Sci. U. S. A. 102 (2005) 6320–6325.
[102] L. Kalvodova, N. Kahya, P. Schwille, R. Ehehalt, P. Verkade, D. Drechsel, K. Simons, Lipids as modulators of proteolytic activity of BACE: involvement of cholesterol, glycosphingolipids, and anionic phospholipids in vitro, J. Biol. Chem. 280 (2005) 36815–36823.
[103] I. Levental, M. Grzybek, K. Simons, Greasing their way: lipid modifications determine protein association with membrane rafts, Biochemistry 49 (2010) 6305–6316.
[104] I. Levental, D. Lingwood, M. Grzybek, U. Coskun, K. Simons, Palmitoylation regulates raft affinity for the majority of integral raft proteins, Proc. Natl. Acad. Sci. U. S. A. 107 (2010) 22050–22054.
[105] D.L. Parton, J.W. Klingelhoefer, M.S.P. Sansom, Aggregation of model membrane proteins, modulated by hydrophobic mismatch, membrane curvature, and protein class, Biophys. J. 101 (2011) 691–699.